POAC'25
St. John's, Newfoundland and Labrador, Canada

Proceedings of the 28th International Conference on Port and Ocean Engineering under Arctic Conditions
Jul 13-17, 2025
St. John's, Newfoundland and Labrador
Canada

Ice loads on wind turbines of a wind farm

Arttu Polojärvi[1], Malith Prasanna[2], Jan Åström[3]
[1] Aalto University, School of Engineering, Department of Energy and Mechanical Engineering, P.O. Box 14100, FI-00076 Aalto, Finland
[2] VTT Technical Research Centre of Finland, P.O. Box 1000, FI-02044 VTT, Finland
[3] CSC – IT Centre for Science Ltd. P.O. Box 405 FI-02101 Espoo, Finland

ABSTRACT

This paper studies level ice loads on offshore wind turbines within a wind farm by using three-dimensional discrete element modeling. Rather than focusing on an individual wind turbine, we investigate simplified scenarios where the ice load on a given turbine in a wind farm is influenced by ice failure processes occurring at other turbines. We focus on a simplified wind farm layout and discuss cases where a turbine can shelter other turbines in its wake. As a part of this analysis, we check how the load may drop at sheltered turbines.

KEY WORDS Offshore wind; Ice loads; Discrete element method.

INTRODUCTION

Due to a strong drive towards renewable energy, plans are underway to install offshore wind farms on sea areas with seasonal ice cover. Offshore wind farms are large structural networks, consisting of up to hundreds of turbines and spanning over sea areas up to hundreds of square kilometers. It remains an active research question how to accurately estimate the ultimate ice loads on a single wind turbine to optimize its foundation structure. Accordingly, earlier work on sea ice behavior on the scale of wind farms has been performed with emphasis on ultimate loads and ice induced vibrations (Kärnä et al., 2010; Hendrikse & Koot, 2019; Gravesen et al., 2023) Even if this is the case, it is also worthwhile asking if ice loading is of equal magnitude on all wind turbines in a wind farm.

The work here is based on discrete element method and focuses on the wind turbines of a simplified wind farm, where the farm has 16 turbines with 1 km spacing in a regular Cartesian grid. We assume an ice field, which initially envelopes the wind farm and then linearly drifts through the farm with a constant velocity. We first present load records on a turbine within the farm and demonstrate how the turbines in the upstream may shelter the ones downstream from the incoming intact ice. Then we discuss the sheltering by analyzing results from simulations with small variations in the angle of drift in relation to the wind farm.

The rest of the paper is organized as follows. We first describe our simulation tool and the simulation set-up. Then we present the relevant results from our simulations and analyze them shortly. After that, we conclude the paper.

METHODS

Discrete element model

The work presented is based on three-dimensional discrete element method (DEM) simulations (Figure 1). We use a DEM code called HiDEM. Originally developed to study brittle fragmentation from a statistical physics perspective, HiDEM was first introduced in (Åström, 2006). In the context of ice, it has been applied to various studies, including glacier calving (Benn and Åström, 2018), ice shelf fracturing (Benn et al., 2022), and sea ice failure and deformation across different scales (Prasanna et al., 2022; Åström et al., 2024; Åström and Polojärvi, 2025).

The representation of sea ice in HiDEM follows an approach commonly used in DEM. Ice is modeled as a lattice of spherical particles connected by Euler-Bernoulli beam elements, which can break under tension or bending as the lattice deforms. This mimics the formation of individual cracks and a consequent localized ice sheet failure. As the cracks merge, they create leads and ice floes. Fracture energy dissipation is captured using a cohesive softening crack model, as described by Prasanna et al. (2022). In this approach, internal forces within a beam gradually decrease to zero as it undergoes failure. As deformation continues, the resulting ice floes interact with each other and with the wind turbines. Particle interactions are governed by a Hertzian contact force, where the force is proportional to the overlap between particles.

Novelty of HiDEM is its design to tackle the computational burden often associated with DEM. The code employs two methods for efficient parallelization: MPI for inter-node communication and OpenMP for intra-node multithreading on multi-core CPUs (Central Processing Units). Alternatively, the code can be compiled with MPI for CPUs to offload intensive computations to GPUs (Graphics Processing Units) using CUDA or HIP. This hybrid coding structure adds complexity, requiring careful optimization to mitigate computational bottlenecks and load imbalances. The simulations in this study were performed on the EuroHPC supercomputer LUMI, which is powered by 10,240 AMD Radeon Instinct MI250X GPUs, delivering a theoretical peak performance exceeding 550 petaflops. In this study, only a small fraction of available resources at LUMI was utilized, leaving substantial potential for scaling up future simulations in both size and duration.

Simulation set-up

In this paper, we examine a scenario as illustrated in Figure 1, where a level ice sheet initially surrounds a wind farm and then begins a linear drift with a constant velocity. The drift occurs at an angle α in relation to the wind farm. The simulations have a simplified wind farm layout consisting of 16 wind turbines arranged in a grid, with turbine spacing L = 1 km. The turbines are equipped with an ice cone, that has a waterline diameter of D = 10 m and a cone angle of 60°. The ice sheet drifts at a velocity of 0.2 m/s, which corresponds to an approximate wind speed of 10 m/s under free drift conditions (Leppäranta, 2011).

The drift velocity is applied as a far-field boundary condition at the edge of the ice sheet. The ice edges parallel to the drift direction are constrained from moving perpendicular to the ice drift direction to simulate a continuous ice field. The ice thickness in the simulations is 1 m and the dimensions of the ice sheet are 6 km in the drift direction and 6 km perpendicular to it. The sheet is discretized into about 5×10^7 particles connected by about 1.5×10^8 beams. We generated inhomogeneity in the ice sheet by randomly removing 20 % of the beams linking

the particles. The total simulated drift distance was 3 km. Depending on α, the channel behind a turbine may come close or even align with downstream turbines, potentially reducing ice loads acting on them. Our earlier study in Polojärvi et al. (2025) suggests that this occurs only within a narrow range of drift angles. Therefore, in this study, we focus on drift angles in the range of 43–45°.

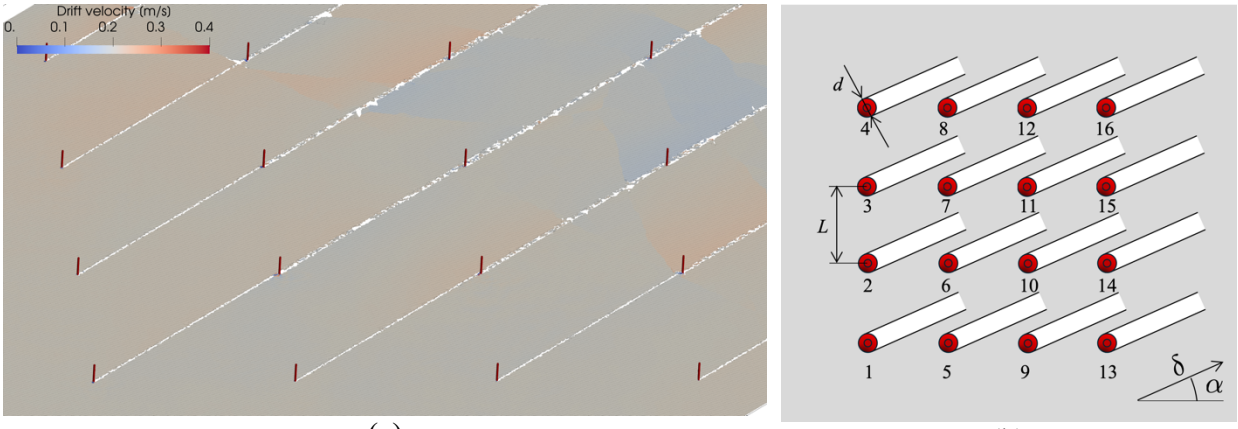

(a) (b)

Figure 1. 16-turbine wind farm simulations: (a) snapshot from a simulation and (b) illustration of the set-up where the angle α of the ice drift δ was varied. The turbines were in a regular grid with L = 1 km spacing. The ice cones had a waterline diameter of d = 10 m. Figure also shows the turbine IDs used in Figures 3a-c.

RESULTS AND DISCUSSION

Ice loads

Figure 2 presents the ice load, F, defined as the sum of horizontal contact forces acting on a turbine inside a 16-turbine wind farm. The load is plotted against the drift distance, δ. The drift angle α = 44.5°. The ice load varies over time, with distinct peaks that occur when ice fragments ride up the ice cone structure. The peak values are limited by the clearing process. We found that the peak load magnitudes were consistent with established estimates. This was determined by comparing the peak load values to the model by Croasdale (2016). Further comparisons to either experimental data or other simulation results could be useful. A significant drop in the ice load levels is observed around $\delta \approx 1400$ m (approximately at $\sqrt{2}\cdot L$). The load drops at the moment when the channel from the upstream turbines reaches the turbines downstream and analyzed below. (When the α = 0° or α = 90°, the drop in the load levels would occur at $\delta \approx 1000$ m = L.) In brief, the upstream turbines start sheltering the analyzed turbines after some time.

Figure 2 further shows the average ice resistance, R, as determined for the turbine as the average ice load experienced by the turbine. Two resistance values were calculated: R_1 representing the average load before the drop, and R_2, representing the average load after the drop. As will be further discussed below, and shown by the results, R_1 was approximately constant for all turbines of the simulated ice field. This suggests that the effect of the modelled ice field inhomogeneity on results was negligible.

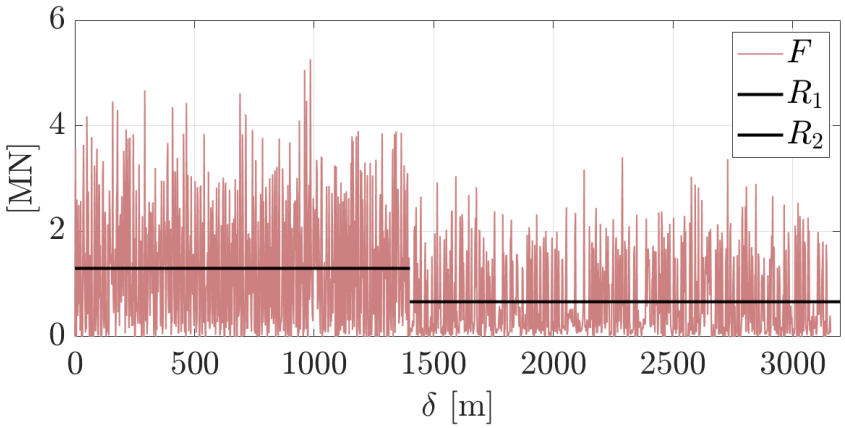

Figure 2. Ice load, F, as a function of drift distance, δ, on a turbine inside the 16-turbine wind farm when drift angle is 45.5°. Load levels exhibit a drop at $\delta \approx 1400$ m. Resistance, R_1 and R_2, were defined as the average ice load before and after the load drop, respectively.

Sheltering

Figure 3 demonstrates how R of the turbines inside the farm changed after the load drop due to the channel of the upstream turbines reaching the downstream turbines. In more detail, Figures 3a-c show the ratio R_2/R_1 for all 16 turbines in simulations with drift angles α = 45°, 44.5° and 43.5°, respectively. Comparison of the three figures immediately shows that the turbines on the perimeter of the farm and facing the incoming ice expectedly always have $R_2/R_1 \approx 1$, whereas the turbines downstream from them see a load drop with $\alpha = 45 \pm 3°$. When α = 45° (Figure 3a), the resistance drops to about 5 % of the initial resistance due to sheltering effect of the upstream turbines, whereas with α = 44.5° the load drop is about 50 % and with α = 43.5° about 20 %. Similar effect would be detected with α = 0° and α = 90° as well.

The behavior of turbines within the group of those at the perimeter of the wind farm and facing incoming ice and within the group of those downstream from them were very similar, as reflected by nearly constant respective R_2/R_1 ratios. The scatter in R_2/R_1 ratios was about 20 % at maximum, and in general within 10 %. This means that the occasional rather complex ice dynamics phenomena—for example, open channels behind turbines being connected by a crack and consequent slow in-plane rotation of resulting floes—seen inside the farm in this simplified setting did not have a major effect on loading of individual turbines.

How to explain the R_2/R_1 ratios in Figure 3? Before the load drop, all turbines in all simulations showed the above-described loading process, further illustrated by the simulation snapshot in Figure 4a. As the figure shows, ice fragments break off from the intact ice sheet due to bending failure and ride up the face of the cone. Once the ride up is high enough, or the incoming ice sheet cannot support the ice mass riding up the cone, clearing occurs. Figure 4b describes the process on the turbines downstream. One reason for load drop is the fact that the bending failure-dominated ice failure process is disturbed by the channel close to the turbine, with some of the cracks in the vicinity of the turbine connecting to the channel. The channels made by the upstream turbines were initially open right behind the turbine, but slowly partially filled with ice fragments broken off the ice sheet. Thus, the turbines downstream also experience loading due to impact-like contacts and small ride-ups of the ice fragments floating with the moving ice sheet.

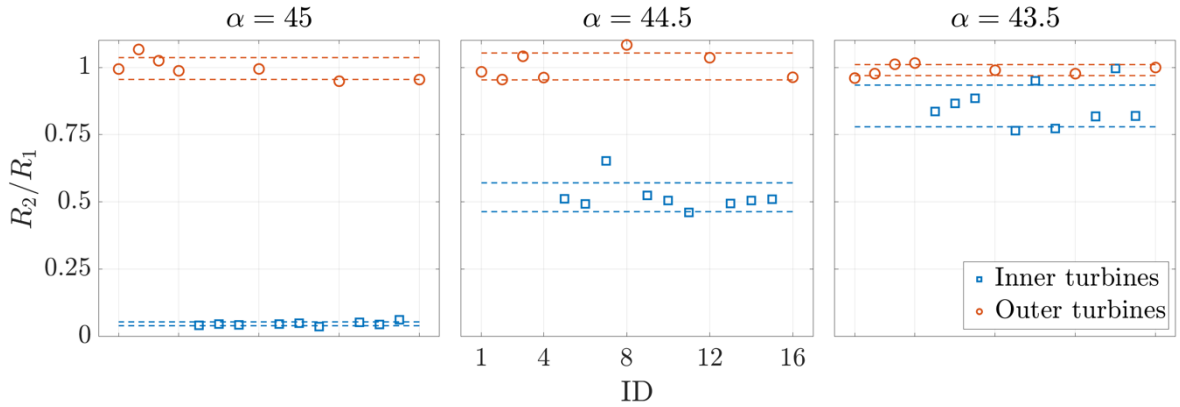

Figure 3. Ratio of resistances R_2 and R_1 before and after the load drop with drift angles (a) α = 45°, (b) α = 44.5° and (c) α = 43.5°.

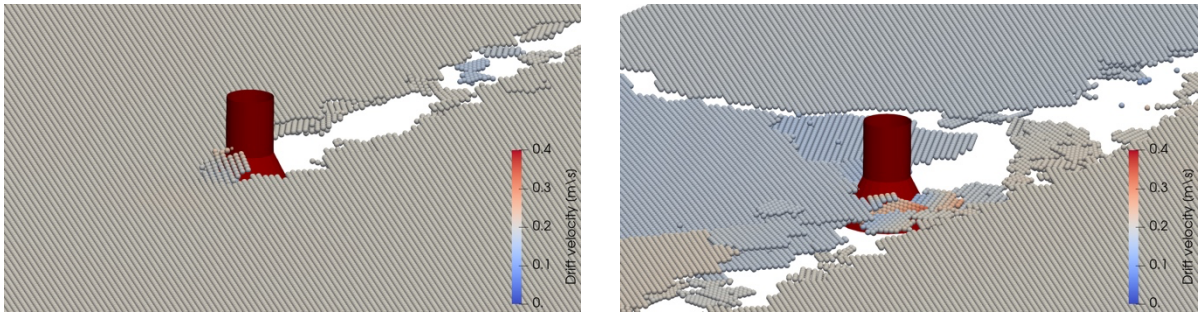

(a) (b)

Figure 4. Ice loading process on a turbine inside the 16-turbine farm (a) before the load drop and (b) after the drop. Here the drift angle α = 44.5°, but the process before the load drop was very similar for all α tested.

Overall, the sheltering effect of the upstream turbines appears to vanish rapidly when α deviates from 45° (this would apply for α = 0° and α = 90° as well). It should anyhow be also noticed that the wind farm we analyzed was rather small and when the farm size increases, the probability of the load drops of the turbines away from the perimeter facing the incoming ice increases. Similarly, the ratio of the turbine spacing and waterline diameter of the structure influences this tendency. Analyzing in detail how this probability changes with the farm and structure size is outside of the scope of this paper. One should also account for the fact that the scenario modelled here is rather simplified, which we think leads to less pronounced interaction effects between the turbines that a more complicated external driving of the ice motion would have caused. Also, if accounted for deformed ice, it would be likely we would observe stronger effects yielded by the turbine ensemble. These two features are likely the source of largest uncertainties in our simulations.

CONCLUSIONS

This study investigated level ice loads on wind turbines within a simplified setting where a wind farm consisting of 16 turbines was arranged in a regular grid. We modeled an intact ice field initially enveloping the farm and drifting through it linearly at a constant velocity. Load records from individual turbines revealed that upstream turbines can produce a sheltering effect, reducing ice loads on downstream turbines. This sheltering effect was further examined by simulating small variations in the ice drift angle relative to the wind farm layout. The results highlighted how even slight changes in drift direction can significantly influence

load distribution across the farm. Inhomogeneity of the ice field and ice dynamics within the wind farm did not have a major effect on the ice loading processes and average loads on the turbines. To further investigate the potential importance of inhomogeneity, future simulations could be performed with ice sheets with greater inhomogeneity or with spatially varying inhomogeneity across the ice sheet.

ACKNOWLEDGEMENTS

AP and MP acknowledge the funding from the European Union – NextGenerationEU instrument through Academy of Finland under grant number (348586) WindySea - Modelling engine to design, assess environmental impacts, and operate wind farms for ice-covered waters. JÅ was supported by the NOCOS DT project, funded by the Nordic Council of Ministers.

REFERENCES

Åström, J., Robertsen, F., Haapala, J., Polojärvi, A., Uiboupin, R., & Maljutenko, I. (2024). A large-scale high-resolution numerical model for sea- ice fragmentation dynamics. The Cryosphere, 18(5), 2429–2442.

Åström, J. A. (2006). Statistical models of brittle fragmentation. Advances in Physics, 54(3–4), 247–278.

Åström, J. A., & Polojärvi, A. (2025). High-resolution fracture dynamics simulation of pack-ice and drift-ice formation during sea ice break up events using the HiDEM2.0 code. Geophysical Research Letters, 51, e2024GL110552.

Benn, D. I., & Åström, J. A. (2018). Calving glaciers and ice shelves. Advances in Physics X, 3(1), 1513819.

Benn, D. I., Luckman, A., Åström, J. A., Crawford, A. J., Cornford, S. L., Bevan, S. L., et al. (2022). Rapid fragmentation of thwaites eastern ice shelf. The Cryosphere, 16(6), 2545–2564.

Croasdale, K., Brown, T., Wong, C., Shrestha, N., Li, G., Spring, W., & Thijssen, J. (2016). Improved equations for the actions of thick level ice on sloping platforms. In Proceedings of the arctic technology conference 2016.

Gravesen, H., Jørgensen, L. B., Høyland, K. V., & Bicker, S. (2023). Simulation of multi-modal vibrations due to ice actions. In Proceedings of the 27th international conference on port and ocean engineering under arctic conditions (POAC'23). Glasgow, United Kingdom, 12-16 June.

Hendrikse, H., & Koot, J. (2019). Consideration of ice drift in determining the contribution of ice-induced vibrations to structural fatigue. In Proceedings of the 25th international conference on port and ocean engineering under arctic conditions (POAC'19). June 9-13, Delft, The Netherlands.

Kärnä, T., Gravesen, H., Fransson, L., & Løset, S. (2010). Simulation of multi- modal vibrations due to ice actions. In Proceedings of the 20th IAHR international manuscript symposium on ice. Lahti, Finland, June 12-18.

Leppäranta, M. (2011). The drift of sea ice. Springer Science & Business Media.

Polojärvi, A, Prasanna, M., & Åström, J. (2025). Level ice resistance of a wind farm: wind turbines as pinning points for sea ice drift. Geophysical Research Letters (under review).

Prasanna, M., Polojärvi, A., Wei, M., & Åström, J. (2022). Modeling ice block failure within drift ice and ice rubble. Physical Review A, 105(4), 045001.